Journal of Alloys and Compounds 512 (2012) 241–245

Contents lists available at SciVerse ScienceDirect

Journal of Alloys and Compounds

journal homepage: www.elsevier.com/locate/jallcom

Microstructure and mechanical properties of a spray-formed Ti-based metallic glass former alloy

Enhuai Yin [a], Longchao Zhuo [a], Bin Yang [b], Hui Wang [a], Tao Zhang [a,*]

[a] Key Laboratory of Aerospace Materials and Performance (Ministry of Education), Department of Materials Science and Engineering, Beihang University, Beijing 100191, China
[b] State Key Laboratory for Advanced Metals and Materials. University of Science and Technology Beijing, Beijing 100083, China

ARTICLE INFO

Article history:
Received 16 June 2011
Received in revised form
15 September 2011
Accepted 16 September 2011
Available online 29 September 2011

Keywords:
Metallic glasses
Rapid solidification
Mechanical properties
Microstructure

ABSTRACT

A $Ti_{45.8}Zr_{6.2}Cu_{39.9}Ni_{5.1}Sn_2Si_1$ composite plate was spray deposited on a copper substrate. From the bottom substrate-contact surface to the upper free surface of the deposit, a layered microstructure evolution in the order of fully amorphous (for the region 1–2 mm perpendicularly away from the substrate), amorphous/nanocrystalline (3–4 mm from the substrate), ultrafine-grained crystalline (5–6 mm from the substrate) and micron-sized crystalline phases (7–8 mm from the substrate) was observed. The oversprayed powders bellow 50 μm exhibit fully amorphous structure, while the ones above 50 μm show certain crystallization behavior. The fracture strength of 1.58–1.85 GPa with obvious plastic strain can be achieved under compressive tests for the spray-formed deposit. Spray forming can therefore produce bulk-sized high strength Ti-based alloy which evolves gradually from certain non-equilibrium towards equilibrium during deposition, which were considered to be attributable to the chill effect at the bottom substrate-contact surface and the following heat entrapment from the successively deposited droplets or powders.

1. Introduction

Over the last decade, Ti-based bulk metallic glasses (BMGs) have gained significant interests in both material science and engineering fields, owing to their unique combination of high specific strength, large elastic limit and good corrosion resistance [1,2]. Several Ti-based BMGs have been developed in Ti(–Zr)–TM–M (TM = Cu, Ni and M = Si, Sn, B) alloy systems, such as Ti–Cu–Ni–B–Si–Sn [3], Ti–Zr–Ni–Cu–Sn [4], and Ti–Zr–Hf–Cu–Ni–Si [5], for which the critical diameters for glass formation were in the range from 1 to 5 mm by copper mold casting method. In addition, Ti-based BMGs with higher glass-forming ability (GFA) such as Ti–Zr–Cu–Ni–Be [6,7] or Ti–Zr–Cu–Pd–Sn [8] have also been reported. However, it is difficult to further improve the GFA of the Ti-based BMGs by traditional copper mold casting method. Therefore, novel rapid solidification techniques should be explored to extend the sample size of Ti-based BMGs.

On the other hand, spray forming [9–15] with the characteristic of rapid solidification, has been developed for the manufacture of near-net shape products. In the spray forming process, high pressure inert gas converts liquid metal stream into variously sized droplets. The subsequent deposition of these droplets, which are a mixture of solid, liquid and partially solidified particles, hits a collector substrate and builds up a solid deposit onto the substrate [9]. A few recent attempts have been made to fabricate amorphous or nanocrystalline Al- [16–19], Mg- [20], Fe- [21,22] and La-based [23] alloys by spray forming. Therefore in this paper, we choose a newly reported Ti-based BMG [24] as the former alloy to study the feasibility of spray forming a bulk material with substantial amorphous phase. The microstructure, thermal properties as well as the mechanical properties of the spray-formed deposit are also studied.

2. Materials and methods

The master alloy with nominal composition was prepared by arc melting pure metals (over 99.9 mass%) in argon atmosphere using a Ti-gettered arc-melter. After that, the master alloy with a total weight of 3.5 kg was remelted under nitrogen atmosphere in a graphite crucible. Then the molten metal was atomized by nitrogen gas into fine droplets, and deposited onto a 60 mm thick copper substrate to form a deposit, during which oversprayed powders not deposited on the substrate were generated. The atomization pressure, flying distance, the ejection temperature and the G/M ratio (the ratio of volumetric gas flow rate to mass of metal flow rate) during spray forming are 0.6 MPa, 600 mm, 1100 K and 8.7 m^3/kg, respectively. The weight of the resultant deposit was about 2.5 kg, and the actual composition of the deposit was measured as 44.43%Ti, 5.78%Zr, 40.99%Cu, 5.31%Ni, 2.09%Sn and 1.40%Si (all in atomic percent). On the other hand, the oversprayed powders were collected and sieved in air, and then classified into three different size ranges: 100–200 μm, 50–100 μm and ≤50 μm. The spray-formed deposit was examined by X-ray diffraction (XRD) using a Bruker AXS D8 X-ray diffractometer with Cu-Kα radiation. Thermal stability of the spray-formed deposit was evaluated by differential scanning calorimeter (DSC) at a heating rate of 0.33 K/s. The backscattered images of polished oversprayed powders and the spray-formed deposit were obtained on

* Corresponding author. Tel.: +86 010 82339705; fax: +86 010 82334869.
E-mail address: zhangtao@buaa.edu.cn (T. Zhang).

0925-8388/$ – see front matter © 2011 Published by Elsevier B.V.
doi:10.1016/j.jallcom.2011.09.074

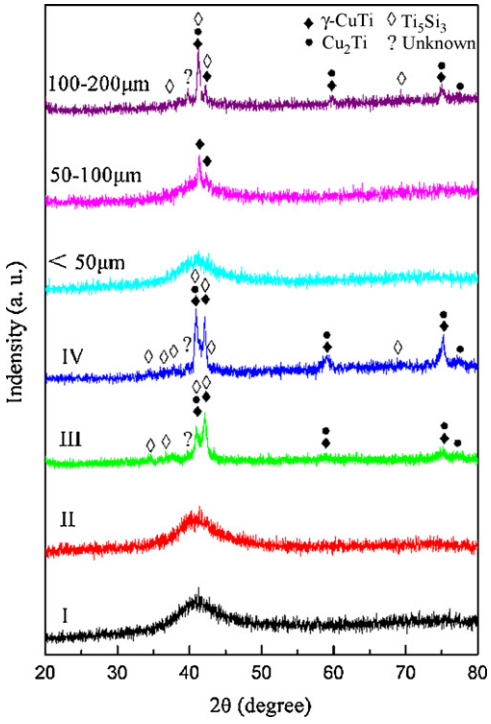

Fig. 1. XRD patterns of oversprayed powders, as well as I, II, III, IV regions of the spray-formed $Ti_{45.8}Zr_{6.2}Cu_{39.9}Ni_{5.1}Sn_2Si_1$ alloy.

JSM-5800 scanning electron microscopy (SEM) equipped with energy dispersive X-ray spectroscopy (EDS). The structure of the deposit was also studied by JEOL 2100F high resolution transmission electron microscope (HRTEM). The samples for TEM observation were prepared by electrochemical polishing with a solution of 4% $HClO_4$ and 96% C_2H_5OH at 243 K. The compressive mechanical properties were measured on SANS testing machine at a constant strain rate of $2.1 \times 10^{-4}\ s^{-1}$. For compression, both ends of the specimens cut from the deposit were polished to make them parallel to each other, and the specimens were 2 mm in diameter and 4 mm in length.

3. Results and discussion

The resultant spray-formed $Ti_{45.8}Zr_{6.2}Cu_{39.9}Ni_{5.1}Sn_2Si_1$ deposit is an irregularly Gaussian-shaped plate with a rough diameter of 300 mm and a maximum thickness of 8 mm. Spray forming makes different microstructure to different areas of the deposit because of different cooling rates during solidification and further thermal treatment from the successively deposited powders or droplets [10]. In order to analyze the structure development, the center, i.e. the maximum thickness of the spray-formed deposit was separated into four regions: I (1–2 mm perpendicularly away from the substrate), II (3–4 mm from the substrate), III (5–6 mm from the substrate) and IV (7–8 mm from the substrate). Fig. 1 shows the XRD patterns of the oversprayed powers with different particle size (≤50 μm, 50–100 μm and 100–200 μm), as well as the cross-section of the samples taken respectively from the above defined four regions. It can be clearly seen that the particles bellow 50 μm exhibit fully amorphous structure, while the ones above 50 μm show certain crystallization behavior. Furthermore, for the powders with the diameter of 50–100 μm, a few spike-like diffraction peaks corresponding to γ-CuTi phase superimpose on the broad amorphous diffraction peak. For the powders with the diameter of 100–200 μm, the sharp diffraction peaks of Cu_2Ti and Ti_5Si_3 phases can be observed besides γ-CuTi. For regions I and II of the deposit, the XRD patterns consists only of a broad peak, with no evidence of any crystalline Bragg peak within the detectable limitation of the XRD. However, with increasing the deposit thickness to the defined region III, some detectable phases such as γ-CuTi, Ti_5Si_3 and Cu_2Ti can be identified. For region IV, more conspicuous diffraction peaks of γ-CuTi, Ti_5Si_3 and Cu_2Ti are observed, indicating the decreasing cooling rate due to the larger distance away from the copper substrate or the more following heat entrapment during the final spray forming process. It should also be mentioned that fully amorphous formation has been obtained up to a thickness of 2 mm for the thinner edged part of the Gaussian-shaped plate.

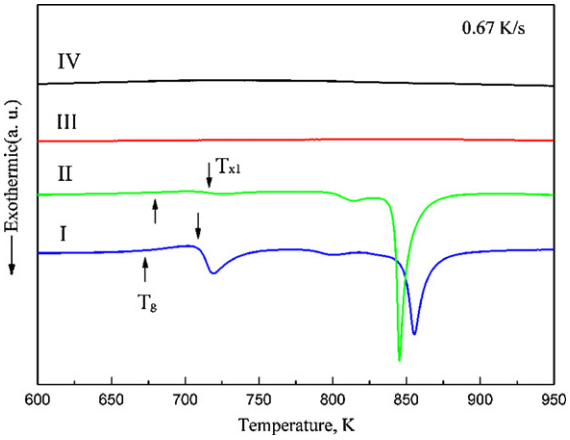

Fig. 2. DSC curves for I, II, III and IV regions of the spray-formed $Ti_{45.8}Zr_{6.2}Cu_{39.9}Ni_{5.1}Sn_2Si_1$ alloy.

In order to further confirm the structure, DSC traces of the samples taken respectively from the four different regions of the deposit are also shown in Fig. 2. For regions I and II, both exhibits an obvious endothermic reaction associated with the glass transition, followed by the supercooled liquid range and then three exothermic reactions due to crystallization. The thermal properties associated with glass transition temperature T_g and first crystallization onset temperature T_{x1} for the fully amorphous region I are 670 K and 710 K, respectively, which are the same as those observed in the as-cast alloy in Ref. [24]. According to the different total enthalpy released from crystallization (105 J/g for region I, and 96 J/g for region II), it can be concluded that the growth or precipitation of some icosahedral clusters or nanocrystalline phases may have taken place. Therefore, the change of composition in the residual amorphous matrix [25] may be the reason for the variation of T_g and T_{x1}, as the arrows marked in Fig. 2. With further increasing the deposit thickness to the labeled regions III and IV, the DSC curves do not show any exothermic reaction, indicating a fully crystalline structure.

The backscattered electron images of polished oversprayed powders are illustrated in Fig. 3(a) and (b). The powders with the diameter lass than 100 μm exhibit a featureless microstructure, indicating that no crystallization has occurred, which is in agreement with the above XRD results. While for the powders larger than 100 μm, the needle-like (black contrast) γ-CuTi and spot-like Ti_5Si_3 crystalline phases (white contrast) have precipitated in the featureless amorphous matrix (grey contrast). Therefore, the critical diameter for the formation of the spherical amorphous phase can be estimated to be around 100 μm under the present experimental processing parameters. Consistent with the XRD results, there is no distinct contrast revealing any micron-sized crystalline phases over the whole cross section of regions I (Fig. 3(c)) and II (Fig. 3(d)). For regions III (Fig. 3(e)) and IV (Fig. 3(f)), it can be seen that γ-CuTi (black contrast) and Ti_5Si_3 (white contrast) crystalline phases cover dominant fraction over the whole cross section according to the EDS and XRD results. Furthermore, it is clear that the average size of the crystalline phases increases from the region III to IV. The novel microstructure feature of the spray-formed deposit may be

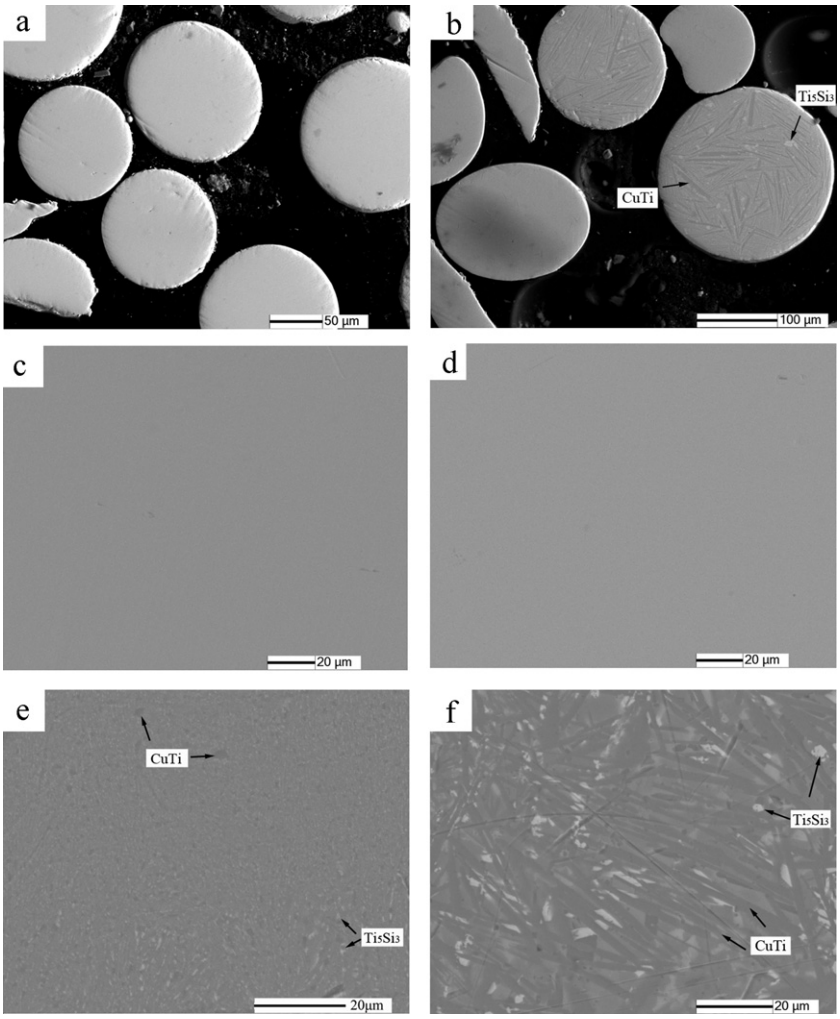

Fig. 3. Backscattered electron images of polished oversprayed powders (a), (b) and the regions I (c), II (d), III (e) and IV (f) of the spray-formed deposit.

therefore attributable to the chill effect at the bottom substrate-contact surface and the following heat entrapment during the deposition of successive layers.

The bright field image with the selected area electron diffraction (SAED) pattern inserted and the HRTEM image for the samples taken from region I are shown in Fig. 4(a) and (b), respectively. The featureless contrast and the broad halo ring indicate its fully amorphous structure. For region II due to the decreasing cooling rate, homogeneously distributed nanocrystallites with an average diameter of ~4 nm are observed in the amorphous matrix according to the HRTEM image, as shown in Fig. 4(c). For region III (Fig. 4(d)), the crystalline phases have precipitated and grown extensively. The nano-sized particles including Cu_2Ti, Ti_5Si_3 and fine strip-shaped γ-CuTi phase (the rectangle in Fig. 4(d) is enlarged as shown in Fig. 4(e)) can be identified. The EDS analysis further reveals that the strips in bright contrast are Ni-depleted phases (close to $Ti_{50}Cu_{50}$), while the ones in dark contrast are Ni-rich phases (close to $Ti_{50}Cu_{37.5}Ni_{12.5}$). For the region IV with the lowest cooling rate during spray forming, the strip-shaped structure has grown and coarsened as shown in Fig. 4(f). The presence of Ti_5Si_3 and Cu_2Ti phases was also confirmed by EDS results, as marked by arrows in Fig. 4(d) and (f).

Fig. 5 shows the compressive engineering stress–strain curves of the samples taken respectively from the four regions of the deposit. The variations of yield strength (σ_y), fracture strength (σ_f) and plastic strain to fracture (ε_p) for each region are summarized in Table 1. It can be seen that the spray-formed deposit exhibits high fracture strength of 1.58–1.85 GPa, with obvious plastic strain of 0.5–10%. It should be noted that, from the bottom substrate-contact surface to the upper free surface of the deposit, there is a tendency of drop in yield strength and rise in plastic strain. For region II, the homogeneously distributed ~4 nm crystallites contribute to the rise in plastic strain in contrast with region I. However, for region III and IV, the appealing properties are similar to that of the in situ

Table 1
Characterization of the samples taken from the four regions of the deposit.

Position	Distance from the substrate (mm)	Microstructure	T_g (K)	T_x (K)	ε (%)	σ_y (GPa)	σ_f (GPa)
I	1–2	Amorphous	670	710	0.5	1.40	1.58
II	3–4	Amorphous + crystalline	680	715	2	1.37	1.63
III	5–6	Ultrafine-grained crystalline	–	–	8	0.82	1.85
IV	7–8	Micron-sized crystalline	–	–	10	0.47	1.66

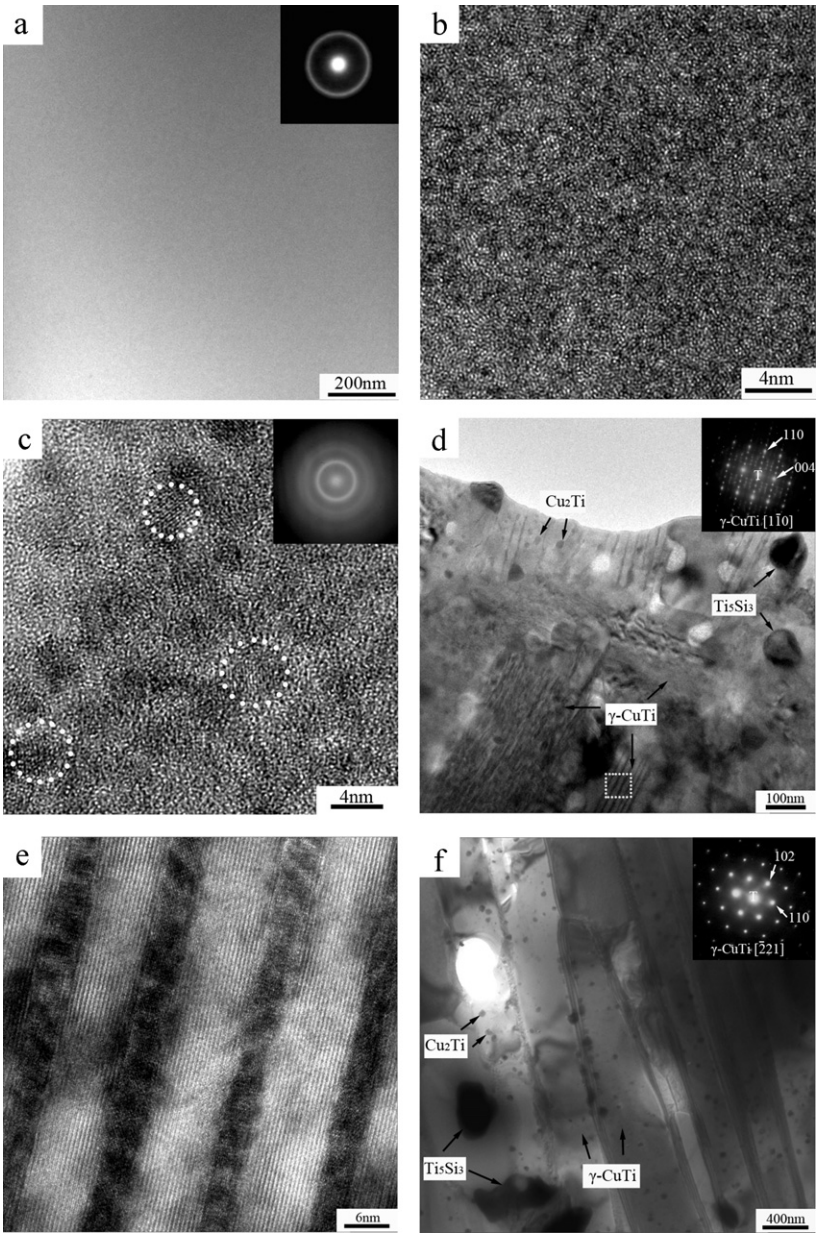

Fig. 4. TEM micrographs with the SAED patterns inserted corresponding to the four regions of the deposit: I (a) (b), II (c), III (d) (e) and IV (f).

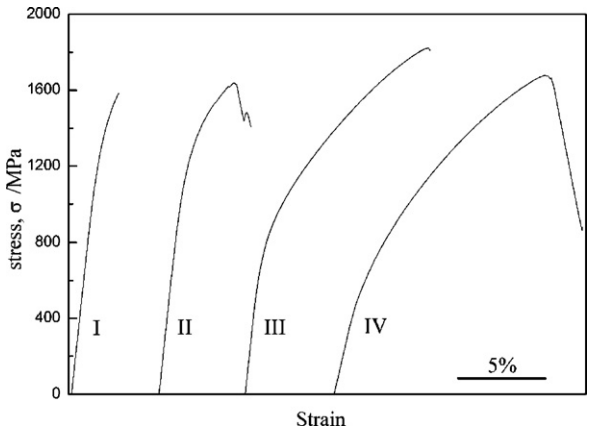

Fig. 5. Compressive stress–strain curves for the four regions of the deposit: I, II, III and IV.

cast heterostructured composites with micrometer-sized dendrites embedded in the matrix of nano-/ultrafine-eutectics, such as in Ti- [26,27], Fe- [28,29], FeCo- [30], Ni- [31] and Al-based [32,33] alloys. It is well known that the deformation of crystalline alloys is strongly dependent on the dislocation activities and dislocation interactions [34]. For regions III and IV, it can be therefore concluded that the ultrafine-grained or micron-sized heterostructured crystalline phases interacted and restricted the localized shear banding, contributing to the large plastic strain under compression.

4. Conclusions

1. A 8 mm thick $Ti_{45.8}Zr_{6.2}Cu_{39.9}Ni_{5.1}Sn_2Si_1$ composite plate was spray deposited on a 60 mm thick copper substrate. From the bottom substrate-contact surface to the upper free surface of the deposit, a layered microstructure evolution in the order of fully amorphous (for the region 1–2 mm perpendicularly away from the substrate), amorphous/nanocrystalline (3–4 mm from

the substrate), ultrafine-grained crystalline (5–6 mm from the substrate) and micron-sized crystalline phases (7–8 mm from the substrate) was observed.
2. The microstructure of the oversprayed powders was also observed. The critical diameter for the formation of the spherical amorphous phase can be estimated to be around 100 μm under the present experimental processing parameters.
3. The fracture strength of 1.58–1.85 GPa with good plastic deformability can be achieved for the spray-formed deposit. The homogeneously distributed nanocrystallites or the ultrafine-grained/micron-sized crystalline phases were considered to have effectively restricted the localized shear banding during compression.

Acknowledgements

This research was financially supported by the National Basic Research Program of China (2007CB613900), National Natural Science Foundation of China (Nos. 50631010, 50671013 and 50771006), and the Innovation Foundation of BUAA for PhD Graduates.

References

[1] A. Inoue, Acta Mater. 48 (2000) 279–306.
[2] B.C. Lu, Y.L. Wang, J. Xu, J. Alloys Compd. 475 (2009) 157–164.
[3] T. Zhang, A. Inoue, Mater. Sci. Eng. A 304–306 (2001) 771–774.
[4] T. Zhang, A. Inoue, Mater. Trans. 39 (1998) 1001–1006.
[5] C.L. Ma, H. Soejima, S. Ishihara, K. Amiya, N. Nishiyama, A. Inoue, Mater. Trans. 45 (2004) 3223–3227.
[6] F.Q. Guo, H.J. Wang, S.J. Poon, G.J. Shiflet, Appl. Phys. Lett. 86 (2005) 091907.
[7] M.Q. Tang, H.F. Zhang, Z.W. Zhu, H.M. Fu, A.M. Wang, H. Li, Z.Q. Hu, J. Mater. Sci. Technol. 26 (2010) 481–486.
[8] S.L. Zhu, X.M. Wang, A. Inoue, Intermetallics 16 (2008) 1031–1035.
[9] P.S. Grant, Prog. Mater. Sci. 39 (4–5) (1995) 497–545.
[10] Y.H. Su, C.Y.A. Tsao, Metall. Mater. Trans. 28B (12) (1997) 1249–1255.
[11] Y.M. Chen, Y.H. Su, R.W. Lin, C.Y.A. Tsao, Acta Mater. 46 (3) (1998) 1011–1023.
[12] W.-J. Kim, J.H. Yeon, J.C. Lee, J. Alloys Compd. 308 (2000) 237–243.
[13] G. Ji, T. Grosdidier, F. Bernard, S. Paris, E. Gaffet, S. Launois, J. Alloys Compd. 434–435 (2000) 358–361.
[14] J.C. Huang, J.P. Chu, J.S.C. Jang, Intermetallics 17 (2009) 973–987.
[15] K. Kaur, O.P. Pandey, J. Alloys Compd. 503 (2010) 410–415.
[16] C.R.M. Afonso, C. Bolfarini, C.S. Kiminami, N.D. Bassim, M.J. Kaufman, M.F. Amateau, T.J. Eden, J.M. Galbraith, Scripta Mater. 44 (2001) 1625–1628.
[17] C.R.M. Afonso, C. Bolfarini, C.S. Kiminami, N.D. Bassim, M.J. Kaufman, M.F. Amateau, T.J. Eden, J.M. Galbraith, J. Non-Cryst. Solid 284 (2001) 134–138.
[18] V.C. Srivastava, K.B. Surreddi, S. Scudino, M. Schowalter, V. Uhlenwinkel, A. Schulz, J. Eckert, A. Rosenauer, H.-W. Zoch, Mater. Sci. Eng. A 527 (2010) 2747–2758.
[19] L.C. Zhuo, B. Yang, H. Wang, T. Zhang, J. Alloys Compd. 509 (2011) L169–L173.
[20] K.F. Chang, M.L.T. Guo, R.H. Kong, Chi.Y.A. Tsao, J.C. Huang, J.S.C. Jang, Mater. Sci. Eng. A 477 (2008) 58–62.
[21] C.R.M. Afonso, C. Bolfarini, W.J. Botta Filho, C.S. Kiminami, Mater. Sci. Eng. A 375–377 (2004) 571–576.
[22] F.L. Catto, T. Yonamine, C.S. Kiminami, C.R.M. Afonso, W.J. Botta, C. Bolfarini, J. Alloys Compd. (2010), doi:10.1016/j.jallcom.2011.02.026.
[23] T.Y. Dong, B. Yang, J.P. He, Y. Zhang, Acta Metall. Sin. 44 (2008) 659–664.
[24] E.H. Yin, M. Zhang, S.J. Pang, X.J. Zhao, T. Zhang, J. Alloys Compd. 504S (2010) S10–S13.
[25] S.C. Glade, J.F. Loffler, S. Bossuyt, W.L. Lohnson, M.K. Miller, J. Appl. Phys. 89 (2001) 1573–1579.
[26] J. Das, K.B. Kim, F. Baier, W. Löser, J. Eckert, Appl. Phys. Lett. 87 (2005) 161907.
[27] J.H. Han, K.B. Kim, S. Yi, J.M. Park, S.W. Sohn, T.E. Kim, D.H. Kim, J. Das, J. Eckert, Appl. Phys. Lett. 93 (2008) 141901.
[28] J.M. Park, S.W. Sohn, T.E. Kim, K.B. Kim, W.T. Kim, D.H. Kim, Scripta Mater. 57 (2007) 1153–1156.
[29] J.M. Park, S.W. Sohn, D.H. Kim, K.B. Kim, W.T. Kim, J. Eckert, Appl. Phys. Lett. 92 (2008) 091910.
[30] R. Li, G. Liu, M. Stoica, J. Eckert, Intermetallics 18 (2010) 134–139.
[31] J.M. Park, T.E. Kim, S.W. Sohn, D.H. Kim, K.B. Kim, W.T. Kim, J. Eckert, Appl. Phys. Lett. 93 (2008) 031903.
[32] J.M. Park, K.B. Kim, D.H. Kim, N. Mattern, R. Li, G. Liu, J. Eckert, Intermetallics 18 (2010) 1829–1833.
[33] L.C. Zhuo, S.J. Pang, H. Wang, T. Zhang, J. Alloys Compd. 504s (2010) S117–S122.
[34] F.R.N. Nabarro, Theory of Crystal Dislocation, Oxford University Press, Oxford, 1967.